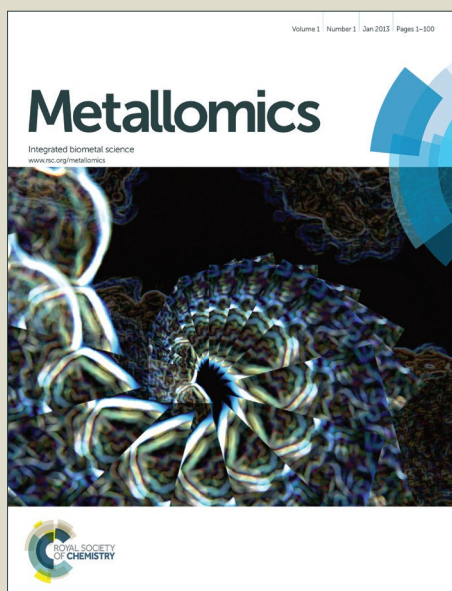


Metallomics

Accepted Manuscript



This is an *Accepted Manuscript*, which has been through the Royal Society of Chemistry peer review process and has been accepted for publication.

Accepted Manuscripts are published online shortly after acceptance, before technical editing, formatting and proof reading. Using this free service, authors can make their results available to the community, in citable form, before we publish the edited article. We will replace this *Accepted Manuscript* with the edited and formatted *Advance Article* as soon as it is available.

You can find more information about *Accepted Manuscripts* in the [Information for Authors](#).

Please note that technical editing may introduce minor changes to the text and/or graphics, which may alter content. The journal's standard [Terms & Conditions](#) and the [Ethical guidelines](#) still apply. In no event shall the Royal Society of Chemistry be held responsible for any errors or omissions in this *Accepted Manuscript* or any consequences arising from the use of any information it contains.

1
2
3
4
5
6
7
8
9
10
11
12
13
14
15
16
17
18
19
20
21
22
23
24
25
26
27
28
29
30
31
32
33
34
35
36
37
38
39
40
41
42
43
44
45
46
47
48
49
50
51
52
53
54
55
56
57
58
59
60

	<p>and Environmental Sciences, Deakin University, Burwood, VIC, Australia Nicholson, Garth ; ANZAC Research Institute, 1. Northcott Neuroscience Laboratory; Molecular Medicine Laboratory, Concord Hospital, Concord, NSW, Australia; Sydney Medical School, University of Sydney, Sydney, NSW, Australia Kennerson, Marina ; Northcott Neuroscience Laboratory, ANZAC Research Institute, Concord, NSW, Australia; Molecular Medicine Laboratory, Concord Hospital, Concord, NSW, Australia; Sydney Medical School, University of Sydney, Sydney, NSW, Australia</p>

SCHOLARONE™
Manuscripts

Metallomics Accepted Manuscript



Metallomics

Characterizing the molecular phenotype of an *Atp7a*^{T985I} conditional knock in mouse model for X-linked distal hereditary motor neuropathy (dHMXN).

Received 00th January 20xx,
Accepted 00th January 20xx

DOI: 10.1039/x0xx00000x

www.rsc.org/metallomics

Gonzalo Perez-Siles^{a,c}, Adrienne Grant^a, Melina Ellis^a, Carolyn Ly^a, Aditi Kidambi^a, Mamdouh Khalil^d, Roxana M. Llanos^e, Sharon La Fontaine^{e,f}, Alleene V. Strickland^g, Stephan Züchner^g, Sandra Bermeo^h, Elysia Neist^h, Tara C. Brennan-Speranza^h, Reinaldo I. Takataⁱ, Carlos E. Speck-Martinsⁱ, Julian F.B. Mercer^e, Garth A. Nicholson^{a,b,c}, Marina L. Kennerson^{a,b,c}.

ATP7A is a P-type ATPase essential for cellular copper (Cu) transport and homeostasis. Loss-of-function *ATP7A* mutations causing systemic Cu deficiency are associated with severe Menkes disease or its milder allelic variant, occipital horn syndrome. We previously identified two rare *ATP7A* missense mutations (P1386S and T994I) leading to a non-fatal form of motor neuron disorder, X-linked distal hereditary motor neuropathy (dHMXN), without overt signs of systemic Cu deficiency. Recent investigations using a tissue specific *Atp7a* knock out model has demonstrated that Cu has an essential role in motor neuron maintenance and function, however the underlying pathogenic mechanisms of *ATP7A* mutations causing axonal degeneration remain unknown. We have generated an *Atp7a* conditional knock in mouse model of dHMXN expressing *Atp7a*^{T985I}, the orthologue of the human *ATP7A*^{T994I} identified in dHMXN patients. Although a degenerative motor phenotype is not observed, the knock in *Atp7a*^{T985I/Y} mice show altered Cu levels within the peripheral and central nervous systems, increased diameter of the muscle fibres and altered *myogenin* and *myostatin* gene expression. *Atp7a*^{T985I/Y} mice have reduced *Atp7a* protein levels and recapitulate the defective trafficking and altered post-translational regulatory mechanisms observed in the human *ATP7A*^{T994I} patient fibroblasts. Our model provides a unique opportunity to characterise the molecular phenotype of dHMXN and the time course of cellular events leading to the process of axonal degeneration in this disease.

Introduction.

Copper (Cu) is a trace element essential for the normal growth and development of all living organisms. In particular, Cu plays a crucial role in the development and function of the central nervous system (CNS) with involvement in processes including neurodevelopment, synaptogenesis, axon extension¹, modulation of neurotransmitter receptor activity and synaptic transmission². Cu dysregulation constitutes a key pathological process in many neurodegenerative disorders, including those where length dependent axonal degeneration occurs such as motor neuron disease (MND)³ and Parkinson's disease^{4,5}. Cu uptake, transport and utilisation are tightly regulated by an integrated network of proteins (reviewed in⁶). Among these proteins is ATP7A, a Cu-

transporting P-type ATPase with a dual role of Cu export across the plasma membrane to maintain Cu homeostasis and providing Cu to Cu-dependent enzymes at the *trans*-Golgi network (TGN). ATP7A executes this dual function through unique trafficking properties. Under normal Cu conditions ATP7A primarily localizes to the TGN. However, when cells are exposed to increased Cu levels, ATP7A traffics to the cell periphery to export the metal from the cell to maintain cellular Cu levels below toxic concentrations⁷⁻⁹.

Mutations in the *ATP7A* gene cause Menkes disease (MD)¹⁰⁻¹² and a milder allelic variant occipital horn syndrome (OHS)¹³. Both of these disorders have similar clinical and biochemical manifestations in which Cu metabolism is severely affected, although neither of the disorders is reported to be associated with motor neuron dysfunction. MD is caused by profound loss-of-function mutations¹⁴⁻¹⁸ whereas OHS is associated with residual Cu transport, often via leaky splice-junction mutations^{13,19} (see review²⁰). We previously identified two missense mutations (T994I and P1386S) in different unrelated families with a form of X-linked hereditary distal motor neuropathy (dHMXN)²¹. This non-fatal form of MND does not have overt signs of systemic Cu-dependent enzyme dysfunction²¹. A mouse model in which the *Atp7a* gene has been selectively knocked out in motor neurons²² has provided important evidence for the role of *Atp7a* and Cu in the maintenance and function of motor neurons. This model however, is unable to elucidate the subtle cellular pathomechanisms of the dHMXN point mutations that lead to axonal degeneration in motor neurons. To more closely mimic the natural disease progression observed in dHMXN patients, we generated an *Atp7a* conditional knock in mouse model of dHMXN

^a Northcott Neuroscience Laboratory, ANZAC Research Institute, Concord, NSW, Australia.

^b Molecular Medicine Laboratory, Concord Hospital, Concord, NSW, Australia.

^c Sydney Medical School, University of Sydney, Sydney, NSW, Australia

^d Molecular Physiology Unit, ANZAC Research Institute, Concord Hospital, The University of Sydney, Sydney, NSW, Australia

^e Centre for Cellular and Molecular Biology, School of Life and Environmental Sciences, Deakin University, Burwood, VIC, Australia.

^f The Florey Institute of Neuroscience and Mental Health, Parkville, Victoria, Australia.

^g Department of Human Genetics, Hussman Institute for Human Genomics, University of Miami Miller School of Medicine, Miami, FL, USA.

^h Discipline of Physiology & Bosch Institute, School of Medical Sciences, University of Sydney, Sydney, NSW, Australia.

ⁱ Sarah Network Rehabilitation Hospitals, Brasilia, DF, Brazil.

(to be known as *Atp7a*^{T985I}). Our model introduces the human *ATP7A*^{T994I} dHMNX mutation into the mouse orthologue. Although a degenerative motor neuropathy phenotype was not observed, we have evidence for nervous system-specific Cu dysregulation, structural and gene expression changes in the muscles from the knock in mice and a molecular phenotype in *Atp7a*^{T985I} primary cells that recapitulate pathogenic cellular events observed in dHMNX patient cells with the T994I mutation. This model represents a unique opportunity to further explore the molecular phenotype of the human disease by examining the time course of early cellular events leading to axonal degeneration in the dHMNX patients.

Materials and methods.

Generation of *Atp7a*^{T985I} knock in mice.

The *Atp7a*^{T985I} knock in mice were generated by Ozgene (Perth, Australia). The dHMNX *ATP7A*^{T994I} mutation was introduced into the mouse *Atp7a* orthologue to generate *Atp7a*^{T985I} using the "mini cDNA" strategy²³. C57BL/6J knock in mice were generated which expressed the wild type cDNA for *Atp7a* exons 15-23 (including a terminating stop codon) which was flanked by lox P sites. Targeted DNA containing the T985I knock in mutation was inserted immediately downstream of the floxed region. These mice were initially crossed with *Flp* deleter knock in mice for *Flp* recombinase mediated removal of the PGK-neo selection marker flanked by the *frt* sequences. Offspring generated minus the PGK-neo cassette were then crossed with OzCre mice (a Cre-deleter line developed by Ozgene) to produce offsprings in which the wild type cDNA is excised and *Atp7a* containing the T985I mutation is expressed from the time of conception. Experimental genotypes included knock in males (*Atp7a*^{T985I/Y}), carrier females (*Atp7a*^{T985I/+}), homozygous females (*Atp7a*^{T985I/T985I}) and wild type males and females (*Atp7a*^{+/+} and *Atp7a*^{-/-}, respectively). The following genotyping primers were designed for testing both the germline target construct transmission as well as genotyping the experimental animals after Cre-lox recombination: P1: CCTACTTCCCGTAAGTGACTCAT; P2: AGTATGAAGGGAGAAACAGCTGAG; P3: AGGATCTCCTGTCATCTCACCT. In the experiments involving mouse embryonic fibroblasts, the sex of the dissected embryos was determined using a previously designed PCR assay to co-amplify the X-chromosome and the Y-chromosome-specific genes, *Jarid1c* and *Jarid1d* respectively,²⁴ using the following primers: mSexF: CTGAAGCTTTGGCTTTGAG and mSexR: CCACTGCCAAATCTTTGG.

Human primary fibroblasts cultures.

Individuals participating in this study provided written consent according to protocols approved by the Sydney Local Health District Human Ethics Review Committee, Concord Repatriation General Hospital, Sydney, Australia (HREC/11/CRGH/105). Primary fibroblasts were cultured from skin biopsies of 3 clinically normal subjects and a dHMNX patient harboring the *ATP7A*^{T994I} mutation. Cultures were maintained in F-DMEM media consisting of DMEM (Gibco, Life technologies) supplemented with 10% (v/v) fetal bovine serum (SAFC Biosciences), 1% (v/v) Penicillin Streptomycin and 1% (v/v) L-glutamine (Gibco, Life technologies) at 37 °C and 5% CO₂.

Mouse embryonic fibroblasts (MEF) cultures.

MEF were derived from day 13.5 embryos (E13.5). Tissue from the embryos was washed with PBS and manually dissociated using a sterile scalpel blade. 1ml of trypsin (0.5% v/v) was added to the

dissociated fetal tissue and the embryo suspension pipetted intensively to obtain a single cell suspension and incubated at 37°C for 20 min. The trypsin was neutralized by adding F-DMEM (6 ml) supplemented with 10% (v/v) MEM Non-Essential Amino Acid Solution (Gibco, Life technologies), mixed and each suspension transferred to a T25 flask and maintained at 37 °C and 5% CO₂.

Western blotting.

Brain and spinal cord were dissected from 6 month old animals and snap frozen in liquid nitrogen. Tissues were homogenized in lysis buffer (10 mM Tris-HCl pH 7.4, 0.1% w/v SDS, 1% v/v Triton X-100, 1X cOmplete, Mini EDTA-free protease inhibitor). Cell lysates were obtained from confluent human fibroblasts (1X10⁶ cells) and MEF (5X10⁵ cells) using RIPA buffer (50 mM Tris-HCl pH 8.0, 150 mM NaCl, 0.1% w/v SDS, 1% v/v Triton X-100, 1% w/v Sodium deoxycholate, 1X cOmplete, Mini EDTA-free protease inhibitor). After protein determination (Pierce BCA Protein Assay Kit, ThermoScientific) 40 µg of tissue homogenates and 15 µg of cell lysates were subjected to SDS-polyacrylamide gel electrophoresis and transferred to polyvinylidene difluoride (PVDF) membranes. Membranes were probed with a rabbit monoclonal ATP7A antibody (Auspep) raised specifically to amino acids of the carboxy-terminus of human ATP7A (1463-DKHSLLVGFREDDDTAL-1480). This sequence is identical to the mouse sequence with the exception of the Ala¹⁴⁷⁹ in human (Thr¹⁴⁹¹ in mouse) and was chosen based on previous studies showing an ATP7A antibody effectively reacting with the rodent *Atp7a*²⁵. Alpha tubulin (SIGMA Aldrich), β-actin (Cell Signaling) and GAPDH (Abcam) antibodies were used as loading controls. Anti-rabbit (SIGMA Aldrich) and anti-mouse (Abcam) horseradish peroxidase (HRP) conjugated secondary antibodies were used and signal detected by adding a chemiluminescent substrate (Merck).

Behavioral tests.

Rotarod.

Mice were trained using a trial run during which the rotarod (LE8200 Accelerating Rota-Rod; SDR Scientific) accelerated from 4 to 40 rpm over 300 s. After this acclimation, mice were timed for three runs on their ability to successfully continue running on the rod and the best performance was used to generate mean scores for each age group and genotype. A fall, a complete rotation, or completion of 300 s ended the run. Breaks (20 min) were given between each run. Data was collected using the *Sedacom* software provided with the instrument.

Hind limb clasping.

Global motor function of the mice was tested with the hind limb clasping function. Weekly, mice were suspended by the tail and the presence of reflexive splaying of the hind limbs and digits in response to elevation was observed and documented.

Histology.

Nerve semi-thin plastic sectioning.

Mice (18 months) were perfused with freshly made 4% (m/v) paraformaldehyde (PFA). Dissected sciatic nerves were post-fixed in 2% (v/v) formaldehyde and 2.5% (v/v) glutaraldehyde overnight at 4°C. Samples were stained in 1% (v/v) osmium tetroxide for 2 h, dehydrated, and then hard-plastic polymer embedded using a mixture of Poly/Bed 812, Araldite 502, dodecylsuccinic anhydride, and dimethylbenzylamine. After hardening overnight at

80–85°C, samples were sliced on a microtome into sections (1 µm) and stained with toluidine blue.

Muscle histology.

Mouse tibialis anterior muscles (24 months) were fixed in 4% (m/v) PFA overnight and embedded in paraffin wax. 5 µm sections were cut and mounted onto glass slides before being dewaxed and stained with hematoxylin and eosin (H&E). Sections were observed with transmission light microscopy on an Olympus BX53 at 20X magnification. *Image J* analysis suite software was used to quantify total and centralized nuclei, as well as fibre diameter.

Myogenin and myostatin mRNA expression.

RNA was extracted from the soleus muscles of the mice (24 months) in Trizol reagent (Life Technologies) with a Kinematica Polytron homogenizer as previously described²⁶. RNA was reverse transcribed using SuperScript III (Life Technologies). The gene expression of *myogenin* and *myostatin* in the soleus muscle was quantified by real time quantitative PCR, using TaqMan® fluorogenic probes and a Sequence Detection System 7000 (Applied Biosystems™/Thermo Fisher Scientific). The $\Delta\Delta C_t$ method²⁷ was used to measure the relative quantitation expression of *myogenin* and *myostatin* and mouse *GAPDH* was used as the housekeeping gene. mRNA from the wild type *Atp7a*^{+Y} mice was chosen as the calibrator sample (i.e. target expression = 1).

Immunofluorescence.

After the indicated treatments outlined in the Results, human fibroblasts or MEF were fixed using 4% (m/v) PFA, for 12 min at room temperature (RT), permeabilized (0.3% (v/v) Triton X-100, 10 min) and blocked (5% (v/v) bovine serum albumin for human cells or 5% (v/v) normal goat serum for MEF, 1 h RT). Cells were incubated with primary antibodies overnight at 4°C and with Alexa Fluor-labeled secondary antibodies (Molecular Probes-Invitrogen, Paisley, UK) at RT for 2 h. Nuclei were counterstained with 300 nM 4,6-diamidino-2-phenylindole (DAPI, Molecular Probes) and mounted using Prolong Gold antifade reagent (Invitrogen). Cells were visualized using a Leica SPE-II confocal microscope and images acquired at 63X magnification. Primary antibodies used include: rabbit monoclonal ATP7A 1:250 (Antibody Solutions) and mouse monoclonal golgin 97 1:500 (CDF4) (Santa Cruz).

Trafficking assay.

Cells were treated with 200 µM CuCl₂ in culture medium for 2 h at 37°C, with the final 30 min in the presence of 50 µg/ml cycloheximide, CHX (SIGMA Aldrich). For the Cu washout, cells were treated with CuCl₂ as described above, washed once with culture medium, and incubated with culture medium containing 50 µg/ml CHX and 200 µM of the Cu-chelating agent bathocuproinedisulfonic acid, BCS (SIGMA Aldrich), for 4 h at 37°C. Addition of the protein synthesis inhibitor CHX ensured only internalized ATP7A/Atp7a was observed after the Cu washout, and not new protein synthesised during the time course of the experiment²⁸. Cells were then processed for immunofluorescence as described above.

Quantification of ATP7A/Atp7a present at the TGN.

For quantification of the ATP7A/Atp7a present at the TGN subsequent to the treatments outlined in the Results, cells were stained with a rabbit monoclonal ATP7A antibody (Antibody Solutions) and a mouse anti-Golgi97 antibody followed by

incubation with an anti-rabbit ALEXA-488 and anti-mouse ALEXA-555 secondary antibodies respectively. Using a Leica SPE-II confocal microscope, settings for optimal visualization of ATP7A/Atp7a at the TGN in control samples and basal conditions were determined and used for the acquisition of all subsequent samples in the experiment. At least 20 images were acquired at 63X magnification for each condition. To precisely define the region on each image corresponding to the TGN and specifically quantify the presence of ATP7A/Atp7a at that location, a region of interest (ROI) was defined using the image processing package *Fiji*²⁹. Briefly, a threshold was applied to the channel containing the TGN information to set appropriate signal-to-noise ratios. By using the “Analyze Particles” option and selecting an appropriate size for the organelle (5–10 µm), the region corresponding to the TGN was outlined in every channel. Using the multi measure option of the ROI master tool, the mean intensity of the signal corresponding to ATP7A/Atp7a was calculated and averaged for every cell.

Cytotoxicity assays.

Cell viability in MEF following a 16 h exposure to increasing concentrations of CuCl₂ was determined with the CCK8 assay kit (SIGMA Aldrich). Briefly, 48 h before the experiment 1.5X10⁴ cells per well were plated in 96 well plates. Prior to the experiment (16 h) the F-DMEM was replaced with fresh media containing the indicated CuCl₂ concentration. Prior to the cytotoxicity assay, cells were washed with DMEM and incubated with CCK8 diluted 1:10 (v/v) in DMEM for 90 min at 37°C. The absorbance at 450nm was measured with an EnSpire Multimode Plate Reader (Perkin Elmer). Data was obtained from 3 independent experiments. The total number of cell lines tested was n = 8 embryos per genotype.

Intracellular metal analysis.

Total intracellular metal content was measured in the *Atp7a*^{T985I} tissues (6 months and 12 months) dissolved in 70% nitric acid as previously described³⁰. Metal content was determined in MEF (*Atp7a*^{+Y} and *Atp7a*^{T985I/Y}) subsequent to the treatments outlined in the Results as previously shown³¹. Briefly, 1X10⁵ cells were seeded in 6 well plates. Cells were grown till confluent and then treated with 200 µM CuCl₂ in culture medium for 16 h at 37°C. For the wash out time points, cells were treated with 200 µM CuCl₂ then media was removed, cells washed with fresh medium and incubated with Cu-free medium for 6 h. After the treatments, cells were harvested and intracellular metal concentration measured using inductively coupled plasma mass spectrometry (ICP-MS, Agilent 7700, Varian). The mean value with standard deviations (± SD) determined in triplicate for each test condition was used for comparison.

Neuromuscular junction (NMJ) analysis.

Preparation and dissection of the distal hind limb lumbrical muscles was performed as described³². Briefly, 24 month old *Atp7a*^{+Y} and *Atp7a*^{T985I/Y} mice were sacrificed, dissected and hind limb lumbrical muscles fixed for 10 min by placing them into a drop of PFA 4% (m/v) at room temperature. All subsequent steps (permeabilization and antibody incubation) were carried out by transferring the muscles through consecutive wells of a clear bottomed 96 well plate at 4°C with agitation. Overnight incubation with the primary antibodies using a 1:100 chicken polyclonal to 68 kDa neurofilament (NF) antibody (Abcam) and a 1:100 mouse monoclonal synaptic vesicle protein 2 (SV2) antibody (DSHB) was performed. Secondary antibodies were incubated for 2 h using 1:250 goat anti-chicken ALEXA Fluor 647 (Abcam) and 1:250 goat

anti-mouse ALEXA Fluor 488 (Molecular Probes) antibodies at 2mg/ml respectively in the dark. To stain postsynaptic acetylcholine receptors (AChR) a conjugated 1:250 α -bungarotoxin peptide-Alexa Fluor-555 was used (Molecular Probes). Lumbrical muscles were mounted using ProLong Gold antifade. Images were analysed as previously described³³ and NMJ occupancy was scored as previously defined³⁴.

Statistical analysis.

For the statistical analysis, 3 independent experiments under the same conditions were performed and a Student's *t* test used to assess the significance of the results. The data are expressed as mean \pm SEM. The following statistical thresholds have been applied throughout the study: * $p < 0.05$; ** $p < 0.01$; *** $p < 0.001$.

Results.

Atp7a^{T985I} mouse generation.

To create a mouse model that would closely mimic the natural disease progression observed in dHMNX patients harboring the *ATP7A*^{T994I} mutation we engineered an *Atp7a*^{T985I} conditional knock in mouse using the "mini cDNA" strategy as previously described²³. The human *ATP7A* and mouse *Atp7a* genes have 89% amino acid identity overall and 100% identity in the TM6 domain where the T985 residue is located³⁵. The targeting strategy for generation of the knock in *Atp7a*^{T985I} mouse model is shown in Fig. 1. A targeting construct (*Atp7a*^{T985I} targeted allele w/neo) was designed to introduce the T985I mutation into exon 15 of the wild type murine *Atp7a* gene (Fig. 1A). By using this strategy, the T985I mutation can be conditionally expressed after removal of the wild type *Atp7a* cDNA following Cre-Lox recombination (knock in *Atp7a*^{T985I}). Germline transmission of the knock in T985I allele was confirmed by a multiplex PCR genotyping assay that co-amplified differential sized DNA fragments detecting the wild type X chromosome and mutant X chromosome containing the T985I mutation (Fig. 1B top panel). The gender of embryos for functional studies were confirmed using the PCR assay designed to co-amplify the X-chromosome and the Y-chromosome-specific homologue genes, *Jarid1c* and *Jarid1d* (Fig. 1B bottom panel).

Reverse transcribed template prepared from brain mRNA was sequenced and confirmed inheritance of the knock in point mutation in the *Atp7a*^{T985I/Y} males (Fig. 1C). Real time quantitative PCR studies did not detect significant differences in *Atp7a* mRNA expression in the brain, spinal cord, sciatic nerve, dorsal root ganglia, liver and skeletal muscle harvested from 6 month old *Atp7a*^{+Y} and *Atp7a*^{T985I/Y} animals (data not shown). However, western blot analysis of tissues from this age group (Fig. 1D) revealed reduced *Atp7a* protein levels in the brain and spinal cord of *Atp7a*^{T985I/Y}, *Atp7a*^{T985I/+} and *Atp7a*^{T985I/T985I} animals when compared to the age matched wild type mice (Fig. 1D').

Behavioral studies and nerve/muscle histology in *Atp7a*^{T985I} aging mice.

Atp7a^{T985I} mice were physically examined on a weekly basis and tested behaviorally for motor abnormalities starting at 4 weeks of age (Fig. 2). The lifespan and the body weight over the course of 2 years were the same in *Atp7a*^{T985I/Y} and *Atp7a*^{+Y} males (Fig. 2A and 2B, respectively) as well as the *Atp7a*^{T985I/+}, *Atp7a*^{T985I/T985I} and

Atp7a^{+Y} females (data not shown). Animals representing all genotypes up to 24 months of age were tested and showed no physical manifestations of peripheral neuropathy as assessed by limb clapping when suspended by the tail (data not shown).

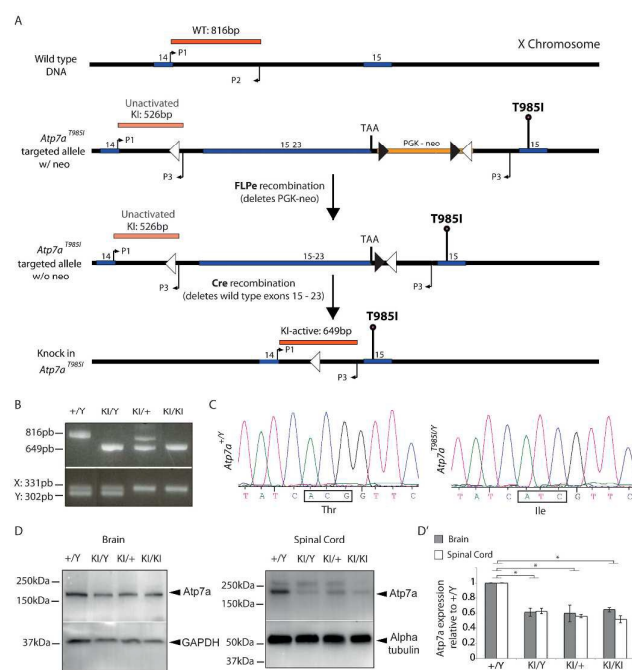


Figure 1. Gene targeting strategy and genotype analysis for *Atp7a*^{T985I} knock in mouse model. (A) Diagram illustrates gene targeting strategy using the mini cDNA approach to produce the *Atp7a*^{T985I} knock in mice. The targeted allele introduces a partial cDNA consisting of the exon to be mutated (exon 15) and all coding downstream exons (16 to 23). The mutated exon 15 (T985I) is inserted downstream of the mini cDNA and the selection marker (PGK-neo). Lox P sites and frt sites are represented by open and closed triangles respectively. FLPe recombination removes the PGK-neo selection marker flanked by the frt sites. Cre-mediated recombination excises the mini cDNA, leaving the T985I mutation and an intronic lox site. P1, P2 and P3 represent primers used for genotyping both the germline target construct transmission as well as genotyping experimental animals after Cre-lox recombination. (B) PCR amplicons (top panel) showing all possible genotypes of the knock in *Atp7a*^{T985I} model: (+/Y) wild type male; (KI/Y) knock in male; (KI/+) carrier females and (KI/KI) homozygous females in E13.5 embryos. The lower panel shows the gender of the embryos based on primers that co-amplify the X chromosome (331 pb) and the Y chromosome-specific (302 pb) genes, *Jarid1c* and *Jarid1d* respectively (C) Partial DNA sequence chromatograms of *Atp7a*^{T985I} reverse transcribed template prepared from brain mRNA obtained from 1 month old mice showing wild type sequence (*Atp7a*^{+Y}) and the mutant sequence (*Atp7a*^{T985I/Y}). (D) Representative western blots showing reduced *Atp7a* protein levels in brain and spinal cord (40 μ g total protein loaded) from 6 month old *Atp7a*^{T985I} mice. Alpha tubulin and GAPDH have been used as the loading control. Quantification of *Atp7a* protein levels is shown (D') and represented as the levels of protein for each genotype relative to the wild type male (+/Y).

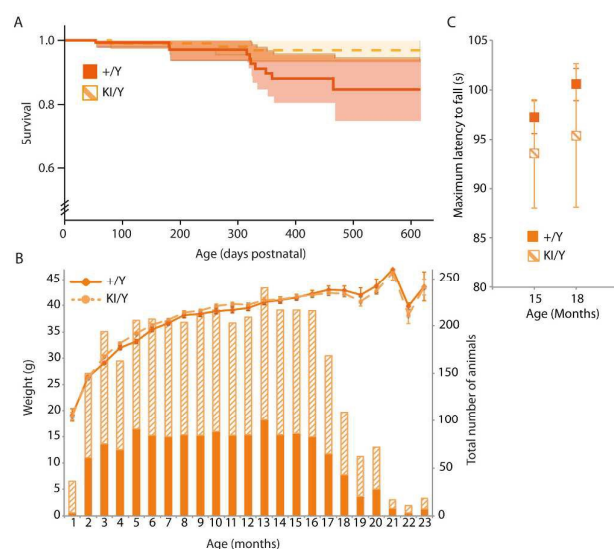


Figure 2. Characterisation of the *Atp7a*^{T985I} mouse phenotype shows no global motor abnormalities. (A) Kaplan Meir survival curves for wild type (+/Y) and knock in (KI/Y) males revealed no significant differences in survival rate between the two groups. (B) Body weight (g) and the total number of animals studied for each age point (months) are shown. (C) Rotarod test at ages 15 (n=35/genotype) and 18 months old (n=16/genotype). The best performance out of three runs for their ability to successfully continue running on an accelerated program (from 4 to 40 rpm over 300 s) was recorded and the mean value for each genotype is shown as the maximum latency to fall.

The motor abilities of *Atp7a*^{T985I/Y} and *Atp7a*^{+Y} mice tested by rotarod performance, showed no statistically significant differences during the timeline of the study (Fig. 2C).

In humans, dHMX causes degeneration of distal portions of peripheral nerves. To examine evidence for axonal degeneration, semi-thin sections of sciatic nerves from 18 month old *Atp7a*^{T985I/Y} and *Atp7a*^{+Y} mice were analysed. We did not observe histological manifestations of acute or chronic neuropathy with light microscopy. Schwann cell changes, missing axons, accumulated membranous debris and clusters of regenerating axons were absent in the nerve preparations. Qualitative analysis of nerves in *Atp7a*^{T985I/Y} mice did not show pathogenic changes in axonal width or myelin thickness when compared to *Atp7a*^{+Y} mice (Fig. 3A).

The neuromuscular junction (NMJ) is a specialised synapse formed between a lower motor neuron and a skeletal muscle fibre and is an early pathological target during axonal degeneration. We therefore investigated the occupancy of NMJ from the hind limb lumbrical muscles of both *Atp7a*^{T985I/Y} and *Atp7a*^{+Y} mice. We stained axonal presynaptic buttons with antibodies against neurofilament (NF) and the synaptic vesicle protein 2 (SV2), as well as the nicotinic acetylcholine receptor (AChR) at the postsynaptic end plate with α -bungarotoxin peptide (Fig. 3B). Neuromuscular synapses were then scored for degenerative phenotypes by assessing the overlap between pre-synaptic SV2/NF and post-synaptic AChR staining, also termed NMJ occupancy (Fig. 3B'). We did not observe any differences in the NMJ occupancy at 24 months. Histological examination of cross sections of tibialis anterior muscles from 24 month old animals (Fig. 3C, top panel) revealed a statistically

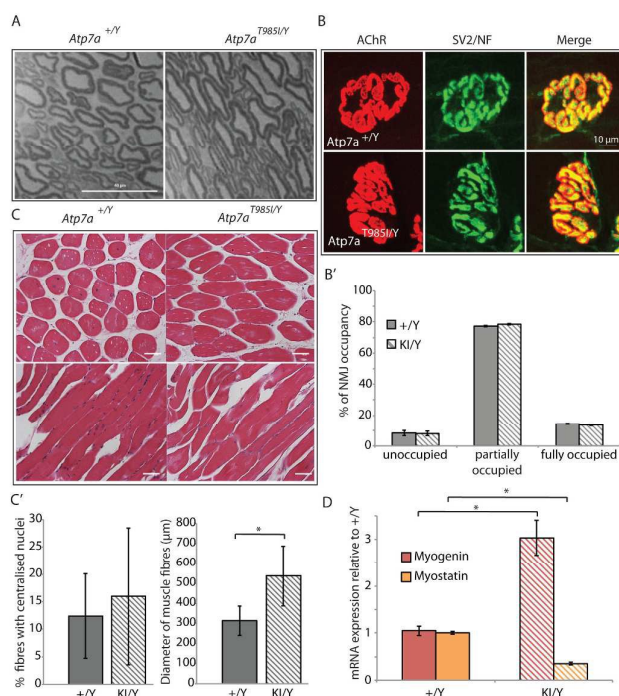


Figure 3. Nerve/muscle histology and NMJ analysis in *Atp7a*^{T985I} aging mice. (A) Microtome sections (1 μ m) from 18 month old *Atp7a*^{T985I/Y} and *Atp7a*^{+Y} sciatic nerves stained with toluidine blue. Scale bar is 40 μ m. (B) NMJ from hind limb lumbrical muscles from 24 month old knock in *Atp7a*^{T985I/Y} (KI/Y) and wild type *Atp7a*^{+Y} (+/Y) mice, stained for post-synaptic (AChR) and pre-synaptic (SV2/NF) structures. The merge panel was used to quantify the NMJ occupancy (B'). Previously defined categories of NMJ percentage occupancy included³⁴: unoccupied (0-33%), partially occupied (34-66%) and fully occupied (67-100%). (C) 5 μ m tibialis anterior sections from 24 month old *Atp7a*^{T985I/Y} and *Atp7a*^{+Y} mice stained with H&E (top panels: cross sections; bottom panels: transverse sections). Stained sections were observed under transmission light at a 20X magnification and quantified (C') for total and centralized nuclei, as well as fibre diameter. (D) Expression analysis of *myogenin* and *myostatin* from reversed transcribed template of soleus muscle by real time quantitative PCR. Mouse *GAPDH* was used to normalize expression of *myogenin* and *myostatin*.

significant increase in the diameter of the *Atp7a*^{T985I/Y} fibres when compared to *Atp7a*^{+Y} fibres (Fig. 3C'). This occurred without changes in the proportion of centralised nuclei between wild type and mutant genotypes (a process found to occur during muscle denervation and atrophy) (Fig. 3C'). Interestingly, transverse sections of the tibialis anterior muscles in the knock in mice showed disorganization of muscle fibres when compared to the wild type (Fig. 3C, bottom panel). Given these unexpected observations we assessed the soleus muscle, the antagonist muscle located in the posterior compartment of the hind limb, for expression of *myogenin* and *myostatin*, genes associated with myogenesis and muscle damage repair^{36, 37}. Gene expression analysis in *Atp7a*^{T985I/Y} soleus muscles using quantitative real time PCR revealed a statistically significant increase of *myogenin* (a muscle-specific transcription factor associated with muscle growth) and reduced expression of *myostatin* (a myogenesis inhibitor) when compared to controls (Fig. 3D).

***Atp7a*^{T985I/Y} mice exhibit nervous system Cu dysregulation.**

We measured Cu concentration in tissues from *Atp7a*^{T985I/Y} and *Atp7a*^{+Y} animals at ages 6 and 12 months (Fig. 4). Our data showed that the brain and spinal cord Cu concentrations were increased in the knock in *Atp7a*^{T985I/Y} mice from the age of 6 months. No statistically significant differences in Cu levels were detected in calf muscle, kidney or liver. A non-significant trend suggested a reduction in the Cu content of the sciatic nerve from *Atp7a*^{T985I/Y} mice when compared to *Atp7a*^{+Y} animals.

Atp7a*^{T985I} primary cells recapitulate molecular defects observed in dHMXN patient derived *ATP7A*^{T994I} fibroblasts.Atp7a* protein levels are reduced in *MEF*^{T985I/Y}.

To further investigate the reduced *Atp7a* protein levels found in the knock in *Atp7a*^{T985I/Y} tissues (Fig. 1D) we measured *ATP7A*/*Atp7a* protein levels in both *ATP7A*^{T994I} patient fibroblasts and MEF isolated from *Atp7a*^{T985I} mice (Fig. 5A). Significantly reduced levels of *Atp7a* in *MEF*^{T985I/Y} compared to *MEF*^{+Y} (Fig. 5A') was observed. A similar decrease in *ATP7A* protein was also detected in *ATP7A*^{T994I} fibroblasts when compared to fibroblasts from clinically normal individuals (Fig. 5A'). These results were further confirmed by immunofluorescence analysis (Fig. 5B). In basal conditions *ATP7A* localizes at the TGN where it supplies Cu to newly synthesized Cu-dependent enzymes. Human control fibroblasts and *MEF*^{+Y} showed

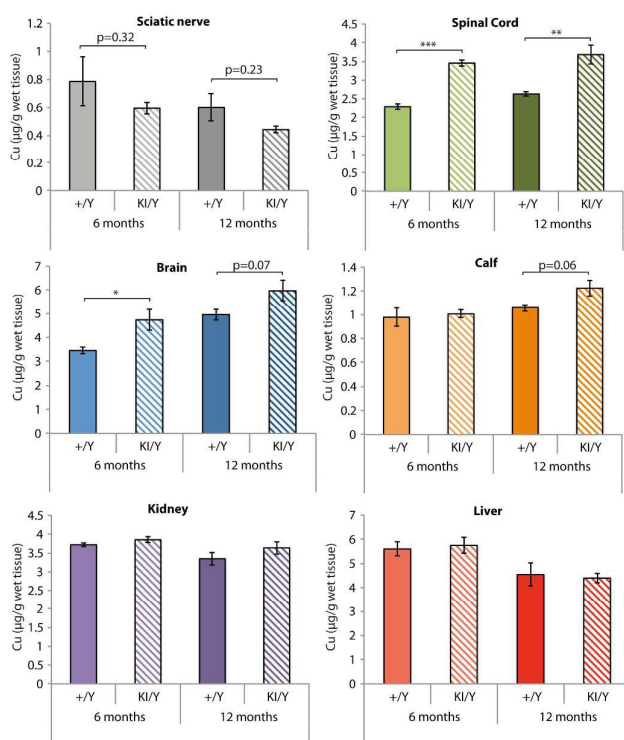


Figure 4. Cu concentrations in wild type and knock in mouse tissues. Cu levels in tissues were determined using ICP-MS at ages 6 (light colors) and 12 months (dark colors) for wild type males (+/Y; solid) and knock in males (KI/Y; striped). The data is represented as the mean ± SEM (n=4 mice/genotype).

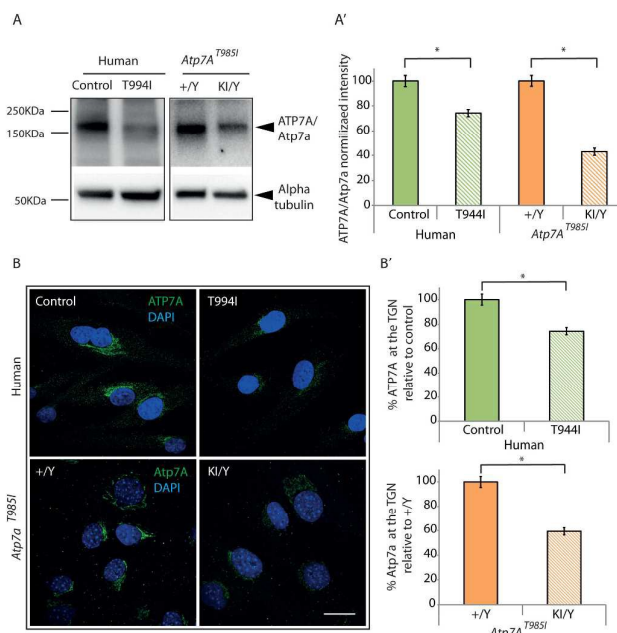


Figure 5. *Atp7a*^{T985I} MEF shows reduced *Atp7a* protein levels as observed in the patient *ATP7A*^{T994I} fibroblasts. Human control fibroblasts (Control), *ATP7A*^{T994I} fibroblasts (T994I) and MEF derived from wild type (+/Y) and knock in (KI/Y) mouse embryos were cultured and *ATP7A*/*Atp7a* protein levels determined with western blot and immunofluorescence analysis. (A) Western blot showing *ATP7A*/*Atp7a* protein levels in the human samples (20 µg) and MEF (15 µg), respectively. Cell lysates probed with an anti-rabbit *ATP7A* antibody show a band at the expected molecular weight (~180 kDa). (A') Alpha tubulin was used as a loading control for normalization and quantitation of the *ATP7A*/*Atp7a* protein levels. (B) Cellular *ATP7A*/*Atp7a* levels were determined by immunofluorescence using a primary rabbit anti-*ATP7A* antibody and an anti-rabbit ALEXA-488 secondary antibody (green). *ATP7A*/*Atp7a* levels were quantitated within the ROI as defined in the methods and are shown relative to the human fibroblasts (Controls) and wild type MEF (+/Y), respectively (B'). Data is obtained from 3 independent experiments (n=50 cells per experiment). Nuclei were stained with DAPI. Scale bar is 20 µm.

strong staining of the Cu transporter at this location. However, the intensity of the *ATP7A*/*Atp7a* staining was significantly decreased in both the *ATP7A*^{T994I} fibroblasts (30% reduction) and *Atp7a*^{T985I/Y} MEF (40% reduction) (Fig 5B').

Atp7a trafficking is impaired in *MEF*^{T985I/Y}.

Exposing cells to elevated levels of Cu induces *ATP7A* to traffic out of the TGN to the cell surface to mediate exporting cellular Cu²⁺. This relocalisation is reversible and upon Cu washout *ATP7A* returns to the TGN^{9, 28}. Previous studies have suggested *ATP7A* trafficking abnormalities occurring in the dHMXN *ATP7A* mutants^{21, 38}. We therefore monitored *ATP7A*/*Atp7a* Cu dependent trafficking in patient *ATP7A*^{T994I} fibroblasts and *Atp7a*^{T985I} MEF, using immunofluorescence and confocal microscopy (Fig. 6A, B). In the presence of the Cu chelator BCS, control cells (human control fibroblasts and *MEF*^{+Y}) show *ATP7A*/*Atp7a* localizing at the TGN. In contrast, the dHMXN *ATP7A*^{T994I} fibroblasts and *MEF*^{T985I/Y} confirmed

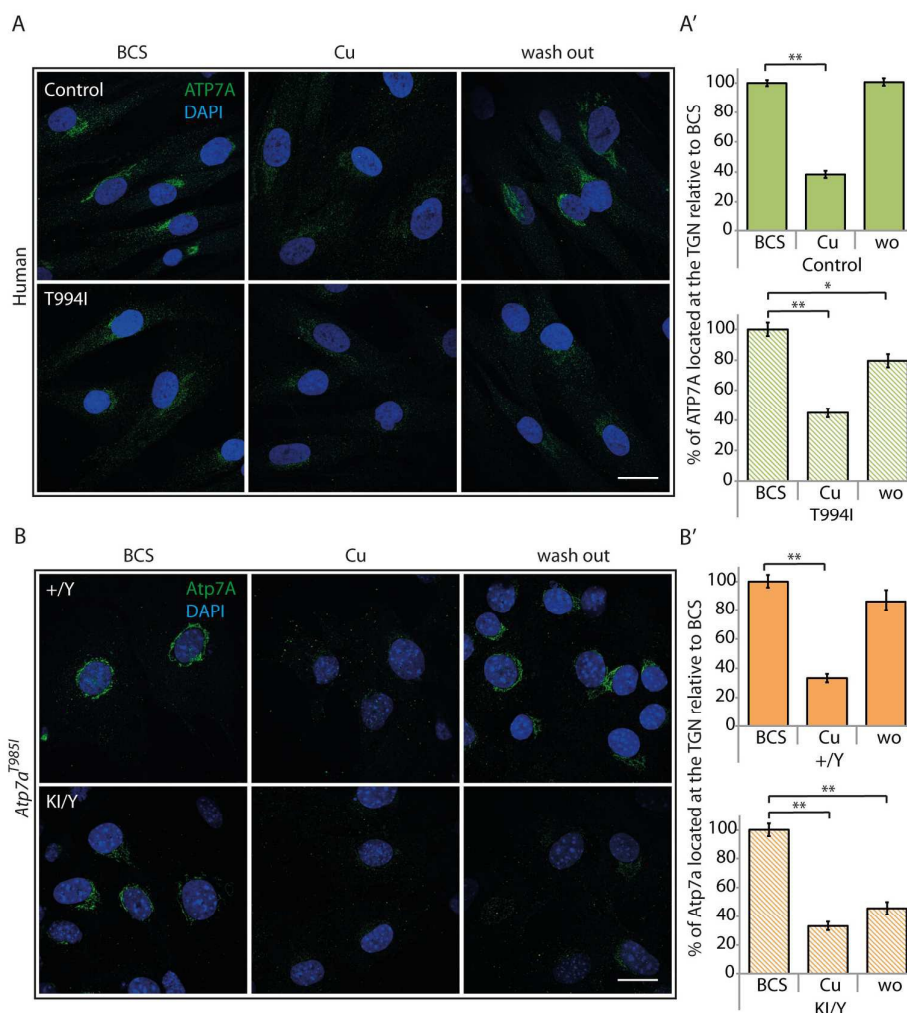


Figure 6. Defective relocation of ATP7A/Atp7a to the TGN is observed in both $ATP7A^{T994I}$ human fibroblasts and $Atp7a^{T985I/Y}$ MEF. (A) Human control (Control) and $ATP7A^{T994I}$ fibroblasts (T994I) and (B) MEF derived from wild type (+/Y) and knock in (KI/Y) mouse embryos were cultured to assess ATP7A/Atp7a intracellular localisation under the following conditions: BCS; cells treated with the Cu-chelating agent at 200 μ M for 2 h. Cu; cells treated with 200 μ M $CuCl_2$ in culture medium for 2h and Cu washout (wo); cells treated with 200 μ M $CuCl_2$, then washed once and incubated with medium containing 50 μ g/ml CHX and 200 μ M BCS for 2 h. Levels within the ROI as described in the methods for ATP7A (A') and Atp7a (B') were quantified for each condition. The mean fluorescence intensity is shown relative to the BCS condition for each genotype. Data was obtained from 3 independent experiments with $n = 50$ cells per experiment. Nuclei were stained with DAPI. Scale bar is 20 μ m.

a ~30% reduction of protein staining at the TGN in these conditions as demonstrated above (Fig. 5). When the cells were exposed to 200 μ M $CuCl_2$ for 2 h only a residual proportion of the initial ATP7A was found at the TGN⁷ in all the cell lines tested, indicating that the dHMNX mutation does not affect trafficking of ATP7A/Atp7a out of the TGN in response to Cu. Quantitation of the fluorescence signal of cells after the Cu wash out showed defective relocation of ATP7A/Atp7a back to the TGN in $ATP7A^{T994I}$ patient fibroblasts (~20% reduction, Fig. 6A') and $MEF^{T985I/Y}$ (~50%, Fig. 6B'). Whether the ATP7A/Atp7a retrograde trafficking is affected by the dHMNX mutation or a defect in the mutant protein causes ATP7A/Atp7a to be retained at alternative intracellular locations after Cu exposure remains to be determined. However, this data confirms that the

$Atp7a^{T985I}$ knock in mouse reproduces the molecular observations made in the $ATP7A^{T994I}$ patient fibroblasts.

Cu does not stabilize Atp7a protein in $MEF^{T985I/Y}$.

Recent investigations have shown a novel post-translational mechanism of Atp7a regulation through stabilisation of the protein by Cu³⁹. Evidence found using rat intestinal epithelial cells (IEC-6) suggested that intracellular Cu accumulation increased steady-state Atp7a protein levels through binding of Cu to one or more of the intracellular Cu-binding domains. We therefore designed experiments to assess the response of Cu loading on ATP7A/Atp7a protein levels in both $ATP7A^{T994I}$ fibroblasts and MEF^{T985I} to determine the effect of the mutation on this process. Human $ATP7A^{T994I}$ and MEF^{T985I} were treated with 200 μ M $CuCl_2$ for 16 h.

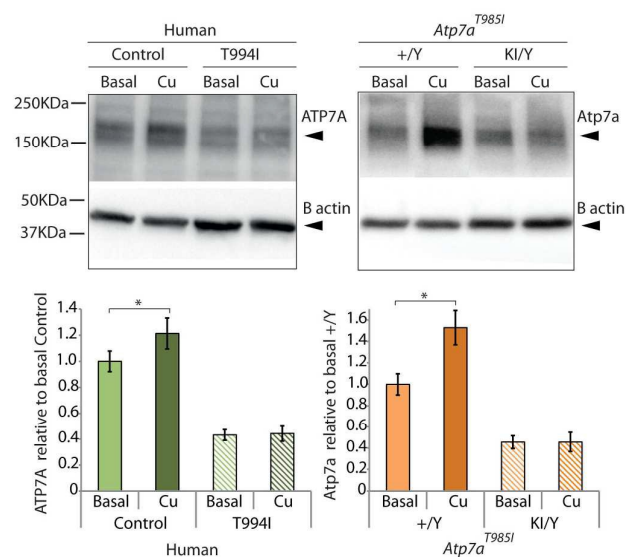


Figure 7. Cu loading increases ATP7A/Atp7a protein levels in control cells but has no effect on ATP7A^{T994I} fibroblasts or Atp7a^{T985I/Y} MEF. Human control fibroblasts (Control), ATP7A^{T994I} patient fibroblasts (T994I) and MEF derived from wild type (+/Y) and knock in (KI/Y) mouse embryos were cultured to assess the effect of Cu loading on cellular ATP7A/Atp7a protein levels. Cells were incubated with 200 μM CuCl₂ for 16 h. Cell lysates (20 μg protein per lane) probed with an anti-rabbit ATP7A antibody showed a band at the expected molecular weight (~180 kDa). β-actin was used as a loading control. ATP7A/Atp7a protein levels for each condition are represented relative to the protein levels detected for the human fibroblasts (Control) or the wild type MEF (+/Y) respectively under basal Cu conditions.

Western blot analysis (Fig. 7) confirmed that exposure of the cells to Cu, increased ATP7A/Atp7a protein levels in control human fibroblasts (20%) and MEF^{+Y} cells (40%). Interestingly, this effect was absent in both the ATP7A^{T994I} patient fibroblasts and the Atp7a^{T985I/Y} MEF. In both cases the ATP7A/Atp7a levels were maintained after Cu loading. This result suggests the ATP7A^{T994I} mutation abolishes ATP7a stabilisation in the presence of excess Cu and confirms that the Atp7a^{T985I} knock in mouse recapitulates this cellular event observed in the patient cells.

MEF^{T985I/Y} accumulate intracellular Cu and are more sensitive to Cu-induced toxicity.

Central to the role of ATP7A within cells is the capacity to traffic to the PM in response to Cu for export and to maintain intracellular levels below toxic concentrations. We propose that the post-translational mechanism for ATP7A regulation examined in our study may have a role in ensuring the cell can effectively restore Cu to physiological levels by increasing the half-life and enhancing the stability of the transporter after Cu insult. The absence of an increase in ATP7A/Atp7a protein levels in both the human and mouse mutant cell lines exposed to elevated Cu therefore suggests that maintenance of intracellular Cu homeostasis may be affected in the ATP7A^{T994I} patient fibroblasts and MEF^{T985I/Y}.

Using ICP-MS we determined intracellular Cu concentrations in Atp7a^{T985I} MEF cultured in basal, Cu loading and Cu-free culture media after exposure to Cu (wash out). Both MEF^{+Y} and MEF^{T985I/Y}

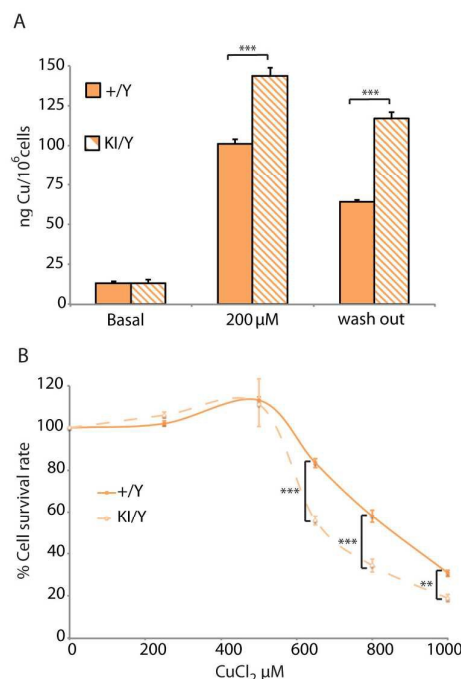


Figure 8. Knock in Atp7a^{T985I/Y} MEF accumulate higher Cu levels and show increased Cu-induced toxicity. (A) Wild type (+/Y) and knock in (KI/Y) MEF were treated with basal medium or 200 μM CuCl₂ for 16 h at 37°C. For the wash out cells were treated with 200 μM CuCl₂ for 16 h and then transferred to Cu-free medium for 6 h. Cu content of cell pellets was measured in triplicate by ICP-MS. Data are expressed as the mean ± SEM for three independent experiments (n=3 embryos/genotype). (B) CCK-8 toxicity assay to determine concentration-dependent Cu toxicity on Atp7a^{T985I} MEF. Wild type (+/Y) and knock in (KI/Y) MEF were exposed to a range of CuCl₂ concentrations from 0 μM to 1000 μM. After 16 h, CuCl₂ containing media was removed and replaced with a solution of 1:10 CCK-8 reagent in fresh DMEM and incubated for 4 h. Absorbance readings at 450nm were recorded and cell survival curves represented relative to the data obtained in the absence of CuCl₂. The data was obtained from 3 independent experiments and represented as the mean ± SEM (n=8 embryos/genotype).

cells showed increased intracellular Cu when exposed to 200 μM CuCl₂ for 16 h. The MEF^{T985I/Y} had a significantly higher cellular Cu accumulation after Cu loading than the wild type MEF^{+Y} (Fig. 8A). After restoration to a Cu free culture media (6 h), MEF^{+Y} were more efficient at reducing the intracellular Cu concentration than the MEF^{T985I/Y}.

These results suggest the dysregulation of Cu homeostasis may therefore be a pathological mechanism underlying the dHMNX ATP7A^{T994I} mutation. To determine whether the Atp7a^{T985I} mutation enhances the cytotoxic effect of Cu, we assessed Cu-induced toxicity for Atp7a^{T985I} MEF, using a Cell Counting Kit-8 (CCK-8) assay to quantify viable cells. MEF^{T985I} showed a dose dependent Cu toxic effect (Fig. 8B) at concentrations over 500 μM CuCl₂. Above this concentration, the toxic effect of Cu in the mutant MEF^{T985I/Y} was significantly higher when compared to wild type MEF^{+Y}. This suggests that the altered capacity of mutant cells to regulate intracellular Cu makes them more susceptible to Cu-induced toxicity.

Discussion and conclusions.

The contribution of ATP7A and Cu to neurodevelopment and neurodegeneration has been extensively explored. However the early cellular events leading to axonal degeneration in the dHMNX patients remains poorly understood. We have characterised an Atp7a conditional knock in mouse model of dHMNX (*Atp7a*^{T9851}) and demonstrated important cellular alterations related with the Atp7a and Cu biology which would help to investigate the early molecular and cellular pathogenic events that occur in the dHMNX patients.

We did not observe a global motor phenotype over the course of this study or demonstrate axonal degeneration through histologic examination of sciatic nerves and NMJ analysis. Our data however, consistently demonstrated the *Atp7a*^{T9851} primary MEF reproduced the molecular observations made in the *ATP7A*^{T9941} patient fibroblasts. The juvenile onset of distal muscular atrophy in the dHMNX patients harboring the T9941 mutation²¹ suggests this mutation produces attenuated effects that require years for patients to present with pathological consequences and this would provide a possible rationale for the absence of a global motor phenotype in the *Atp7a*^{T9851} mice. The previously reported *Atp7a*^{MN/Y} mouse model, in which *Atp7a* had been completely knocked out in the motor neurons, only exhibited behavioral abnormalities after 6 months of age²². This suggests the possibility of compensatory processes occurring in mice that would mitigate the absence or pathogenic function of mutant Atp7a within the motor neurons.

In contrast to Menkes disease, where most *ATP7A* mutations lead to a complete loss of function of the transporter (see²⁰ for review), the dHMNX *ATP7A*^{T9941} mutation produces a subtle reduction in *ATP7A* protein levels (30%) that had not been observed in previous studies and was detected in both the *ATP7A*^{T9941} patient fibroblasts and in the mutant *MEF*^{T9851/Y}. Our data also confirmed a previous observation that wild type Atp7a protein levels are increased in the presence of Cu³⁹. Interestingly the *ATP7A*^{T9941} patient fibroblasts and *MEF*^{T9851/Y} lacked this post-translational regulatory mechanism. We therefore proposed the absence of such stabilisation by Cu in the mutant *ATP7A*/*Atp7a* protein would affect the capacity of the cells to maintain intracellular Cu homeostasis. The reduced cell viability observed in the *MEF*^{T9851/Y} in the presence of high concentrations of Cu suggests Cu accumulation as a possible pathogenic mechanism in dHMNX disease. The contribution of Cu toxicity as an underlying pathogenic mechanism for neurodegenerative disorders has been extensively studied and reviewed⁴⁰. The exact mechanism by which Cu triggers axonal degeneration in the dHMNX patient remains to be determined. Deficiency of Cu dependent enzymes as a result of the decreased presence of Atp7a in the TGN (Fig. 5) represents an alternative disease mechanism in dHMNX. Abnormal function of Cu dependent enzymes, including cytochrome c oxidase⁴¹ and superoxide dismutase 1⁴² have been associated with Charcot-Marie-Tooth and amyotrophic lateral sclerosis (ALS), respectively. In addition, Atp7a loss of function at the TGN is consistent with outcomes from the *Atp7a*^{MN/Y} mice in which the degenerative motor neuropathy of the animals is associated with an overall decrease in Cu in the spinal cord²². Our ICP-MS data showing a non-significant reduction in the levels of Cu in the sciatic nerve of the *Atp7a*^{T9851/Y} mice will need further investigation. Interestingly, assessment of iron levels showed a significant increase in the *Atp7a*^{T9851/Y} sciatic nerves,

whereas no changes were found in any other tissues (Supplementary Fig. S1). Iron accumulation in the CNS is reported in both familial and sporadic forms of ALS³ and the impact of iron mediated toxicity through disruption of mitochondrial iron homeostasis in an ALS mouse model has been described⁴³. The *Atp7a*^{T9851} knock in mouse provides a valuable tool to test the impact of iron on the pathology of dHMNX.

Although no signs of axonal degeneration were observed, the muscle histology revealed an increased diameter of the muscle fibres and signs of disorganized fibre alignment in the *Atp7a*^{T9851/Y} tibialis anterior muscles. Furthermore, gene expression analysis showed significant concomitant increased *myogenin* and reduced *myostatin* gene expression in the *Atp7a*^{T9851/Y} soleus when compared to controls. These observations in the different muscle tissues may reflect a pre-symptomatic stage of the disease we speculate to be associated with enhanced neuronal input occurring in the *Atp7a*^{T9851/Y} muscles at the NMJ. Studies have established that Cu negatively regulates the activity of the NMDA receptors in hippocampal neurons⁴⁴ and the relevance of this regulatory mechanism in synaptic plasticity and excitotoxic cell death has been described⁴⁵. Schlieff et al demonstrated that Cu chelation exacerbates NMDA-mediated excitotoxic cell death via an increased flux of Ca²⁺ into neurons. More recently, NMDA receptors have been found at the postsynaptic end plate of NMJs⁴⁶⁻⁴⁸ suggesting a regulatory function of glutamate and NMDA receptors at the vertebrate NMJ. The release of Cu at the end of the nerves may negatively regulate the activity of the muscle in a similar way that has been proven for hippocampal neurons. The increased diameter of the tibialis anterior fibres we report in the *Atp7a*^{T9851/Y} mice may be a sign of muscle hyperactivity due to impaired release of Cu at the NMJ synapse. Although no changes were observed in the nerve pathology (18 months) or NMJ (24 months) analysis in the knock in animals, the increased gene expression of *myogenin* we have observed might also suggest events of muscle repair due to excitotoxicity from muscle hyperactivity. It is plausible that both the reduction of Atp7a protein and trafficking deficits we have reported in the *Atp7a*^{T9851/Y} mice could contribute to this process in the early stages of the disease. Whilst this hypothesis requires further studies in the *Atp7a*^{T9851} knock in model, in humans the NMDA receptor-dependent release of Cu into the NMJ may protect both motor neurons and muscle fibres from Ca²⁺ induced cytotoxicity in clinically normal individuals.

Our study has characterized a knock in *Atp7a*^{T9851} mouse model, which recapitulates at the cellular level important aspects found in the dHMNX patient cells. Our data suggests that the altered capacity of mutant MEF^{T9851/Y} to regulate Cu intracellular levels make them more susceptible to Cu-induced toxicity. Alternative pathological mechanisms such as increased NMDA receptor-mediated excitotoxicity⁴⁵ in dHMNX patients, the occurrence of aberrant protein interactions of the mutant *ATP7A*³⁸ selectively affecting motor neurons or deficiency of cuproenzymes⁴¹ with a critical impact on the peripheral nerves also may contribute to the disease pathomechanism. Further investigations using primary *Atp7a*^{T9851} motor neurons will provide an ideal tool to investigate the proposed disease mechanisms in the relevant cell model for dHMNX.

Acknowledgements.

The authors thank the families. This research was supported by the National Health and Medical Research Council Project Grant (APP1007705) awarded to M.L.K. and G.A.N. and USA Muscular Dystrophy Association Project Grant (MDA217729) awarded to M.L.K. and G.A.N. We dedicate this work to the memory of our colleague and friend Jim Garbern.

References.

- R. El Meskini, K. L. Crabtree, L. B. Cline, R. E. Mains, B. A. Eipper and G. V. Ronnett, ATP7A (Menkes protein) functions in axonal targeting and synaptogenesis, *Molecular and cellular neurosciences*, 2007, **34**, 409-421.
- N. D'Ambrosi and L. Rossi, Copper at synapse: Release, binding and modulation of neurotransmission, *Neurochemistry international*, 2015, **90**, 36-45.
- E. J. Kasarskis, L. Tandon, M. A. Lovell and W. D. Ehmann, Aluminum, calcium, and iron in the spinal cord of patients with sporadic amyotrophic lateral sclerosis using laser microprobe mass spectroscopy: a preliminary study, *Journal of the neurological sciences*, 1995, **130**, 203-208.
- F. Larner, B. Sampson, M. Rehkemper, D. J. Weiss, J. R. Dainty, S. O'Riordan, T. Panetta and P. G. Bain, High precision isotope measurements reveal poor control of copper metabolism in parkinsonism, *Metallomics : integrated biometal science*, 2013, **5**, 125-132.
- S. R. Paik, H. J. Shin, J. H. Lee, C. S. Chang and J. Kim, Copper(II)-induced self-oligomerization of alpha-synuclein, *The Biochemical journal*, 1999, **340 (Pt 3)**, 821-828.
- I. F. Scheiber, J. F. Mercer and R. Dringen, Metabolism and functions of copper in brain, *Progress in neurobiology*, 2014, **116**, 33-57.
- M. J. Petris, J. F. Mercer, J. G. Culvenor, P. Lockhart, P. A. Gleeson and J. Camakaris, Ligand-regulated transport of the Menkes copper P-type ATPase efflux pump from the Golgi apparatus to the plasma membrane: a novel mechanism of regulated trafficking, *The EMBO journal*, 1996, **15**, 6084-6095.
- J. F. Monty, R. M. Llanos, J. F. Mercer and D. R. Kramer, Copper exposure induces trafficking of the menkes protein in intestinal epithelium of ATP7A transgenic mice, *The Journal of nutrition*, 2005, **135**, 2762-2766.
- L. Nyasae, R. Bustos, L. Braiterman, B. Eipper and A. Hubbard, Dynamics of endogenous ATP7A (Menkes protein) in intestinal epithelial cells: copper-dependent redistribution between two intracellular sites, *American journal of physiology. Gastrointestinal and liver physiology*, 2007, **292**, G1181-1194.
- J. Chelly, Z. Tumer, T. Tonnesen, A. Petterson, Y. Ishikawa-Brush, N. Tommerup, N. Horn and A. P. Monaco, Isolation of a candidate gene for Menkes disease that encodes a potential heavy metal binding protein, *Nature genetics*, 1993, **3**, 14-19.
- J. F. Mercer, J. Livingston, B. Hall, J. A. Paynter, C. Begy, S. Chandrasekharappa, P. Lockhart, A. Grimes, M. Bhave, D. Siemieniak and et al., Isolation of a partial candidate gene for Menkes disease by positional cloning, *Nature genetics*, 1993, **3**, 20-25.
- C. Vulpe, B. Levinson, S. Whitney, S. Packman and J. Gitschier, Isolation of a candidate gene for Menkes disease and evidence that it encodes a copper-transporting ATPase, *Nature genetics*, 1993, **3**, 7-13.
- S. G. Kaler, L. K. Gallo, V. K. Proud, A. K. Percy, Y. Mark, N. A. Segal, D. S. Goldstein, C. S. Holmes and W. A. Gahl, Occipital horn syndrome and a mild Menkes phenotype associated with splice site mutations at the MNK locus, *Nature genetics*, 1994, **8**, 195-202.
- S. Das, B. Levinson, S. Whitney, C. Vulpe, S. Packman and J. Gitschier, Diverse mutations in patients with Menkes disease often lead to exon skipping, *American journal of human genetics*, 1994, **55**, 883-889.
- M. P. Moizard, N. Ronce, S. Blesson, E. Bieth, L. Burglen, C. Mignot, I. Mortemousque, N. Marmin, B. Dessay, C. Danesino, F. Feillet, P. Castelneau, A. Toutain, C. Moraine and M. Raynaud, Twenty-five novel mutations including duplications in the ATP7A gene, *Clinical genetics*, 2011, **79**, 243-253.
- Z. Tumer, C. Lund, J. Tolshave, B. Vural, T. Tonnesen and N. Horn, Identification of point mutations in 41 unrelated patients affected with Menkes disease, *American journal of human genetics*, 1997, **60**, 63-71.
- P. C. Liu, P. E. McAndrew and S. G. Kaler, Rapid and robust screening of the Menkes disease/occipital horn syndrome gene, *Genetic testing*, 2002, **6**, 255-260.
- S. G. Kaler, Metabolic and molecular bases of Menkes disease and occipital horn syndrome, *Pediatric and developmental pathology : the official journal of the Society for Pediatric Pathology and the Paediatric Pathology Society*, 1998, **1**, 85-98.
- J. Tang, S. Robertson, K. E. Lem, S. C. Godwin and S. G. Kaler, Functional copper transport explains neurologic sparing in occipital horn syndrome, *Genetics in medicine : official journal of the American College of Medical Genetics*, 2006, **8**, 711-718.
- Z. Tumer, An overview and update of ATP7A mutations leading to Menkes disease and occipital horn syndrome, *Human mutation*, 2013, **34**, 417-429.
- M. L. Kennerson, G. A. Nicholson, S. G. Kaler, B. Kowalski, J. F. Mercer, J. Tang, R. M. Llanos, S. Chu, R. I. Takata, C. E. Speck-Martins, J. Baets, L. Almeida-Souza, D. Fischer, V. Timmerman, P. E. Taylor, S. S. Scherer, T. A. Ferguson, T. D. Bird, P. De Jonghe, S. M. Feely, M. E. Shy and J. Y. Garbern, Missense mutations in the copper transporter gene ATP7A cause X-linked distal hereditary motor neuropathy, *American journal of human genetics*, 2010, **86**, 343-352.
- V. L. Hodgkinson, J. M. Dale, M. L. Garcia, G. A. Weisman, J. Lee, J. D. Gitlin and M. J. Petris, X-linked spinal muscular atrophy in mice caused by autonomous loss of ATP7A in the motor neuron, *The Journal of pathology*, 2015, **236**, 241-250.
- K. Skvorak, B. Vissel and G. E. Homanics, Production of conditional point mutant knockin mice, *Genesis*, 2006, **44**, 345-353.
- S. J. Clapcote and J. C. Roder, Simplex PCR assay for sex determination in mice, *BioTechniques*, 2005, **38**, 702, 704, 706.

Metallomics

Paper

- 1
2
3
4
5
6
7
8
9
10
11
12
13
14
15
16
17
18
19
20
21
22
23
24
25
26
27
28
29
30
31
32
33
34
35
36
37
38
39
40
41
42
43
44
45
46
47
48
49
50
51
52
53
54
55
56
57
58
59
60
25. T. C. Steveson, G. D. Ciccotosto, X. M. Ma, G. P. Mueller, R. E. Mains and B. A. Eipper, Menkes protein contributes to the function of peptidylglycine alpha-amidating monooxygenase, *Endocrinology*, 2003, **144**, 188-200.
26. T. C. Brennan-Speranza, H. Henneicke, S. J. Gasparini, K. I. Blankenstein, U. Heinevetter, V. C. Cogger, D. Svistounov, Y. Zhang, G. J. Cooney, F. Buttgerit, C. R. Dunstan, C. Gundberg, H. Zhou and M. J. Seibel, Osteoblasts mediate the adverse effects of glucocorticoids on fuel metabolism, *The Journal of clinical investigation*, 2012, **122**, 4172-4189.
27. T. D. Schmittgen and K. J. Livak, Analyzing real-time PCR data by the comparative C(T) method, *Nature protocols*, 2008, **3**, 1101-1108.
28. Z. G. Holloway, R. Grabski, T. Szul, M. L. Styers, J. A. Coventry, A. P. Monaco and E. Sztul, Activation of ADP-ribosylation factor regulates biogenesis of the ATP7A-containing trans-Golgi network compartment and its Cu-induced trafficking, *American journal of physiology. Cell physiology*, 2007, **293**, C1753-1767.
29. J. Schindelin, I. Arganda-Carreras, E. Frise, V. Kaynig, M. Longair, T. Pietzsch, S. Preibisch, C. Rueden, S. Saalfeld, B. Schmid, J. Y. Tinevez, D. J. White, V. Hartenstein, K. Eliceiri, P. Tomancak and A. Cardona, Fiji: an open-source platform for biological-image analysis, *Nature methods*, 2012, **9**, 676-682.
30. V. L. Hodgkinson, S. Zhu, Y. Wang, E. Ladomersky, K. Nickelson, G. A. Weisman, J. Lee, J. D. Gitlin and M. J. Petris, Autonomous requirements of the Menkes disease protein in the nervous system, *American journal of physiology. Cell physiology*, 2015, DOI: 10.1152/ajpcell.00130.2015, ajpcell 00130 02015.
31. M. A. Cater, S. La Fontaine, K. Shield, Y. Deal and J. F. Mercer, ATP7B mediates vesicular sequestration of copper: insight into biliary copper excretion, *Gastroenterology*, 2006, **130**, 493-506.
32. J. N. Sleigh, R. W. Burgess, T. H. Gillingwater and M. Z. Cader, Morphological analysis of neuromuscular junction development and degeneration in rodent lumbrical muscles, *Journal of neuroscience methods*, 2014, **227**, 159-165.
33. N. Tse, M. Morsch, N. Ghazanfari, L. Cole, A. Visvanathan, C. Leamey and W. D. Phillips, The neuromuscular junction: measuring synapse size, fragmentation and changes in synaptic protein density using confocal fluorescence microscopy, *Journal of visualized experiments : JoVE*, 2014, DOI: 10.3791/52220.
34. L. H. Comley, H. R. Fuller, T. M. Wishart, C. A. Mutsaers, D. Thomson, A. K. Wright, R. R. Ribchester, G. E. Morris, S. H. Parson, K. Horsburgh and T. H. Gillingwater, ApoE isoform-specific regulation of regeneration in the peripheral nervous system, *Human molecular genetics*, 2011, **20**, 2406-2421.
35. P. Gourdon, X. Y. Liu, T. Skjorringe, J. P. Morth, L. B. Moller, B. P. Pedersen and P. Nissen, Crystal structure of a copper-transporting PIB-type ATPase, *Nature*, 2011, **475**, 59-64.
36. E. Meadows, J. H. Cho, J. M. Flynn and W. H. Klein, Myogenin regulates a distinct genetic program in adult muscle stem cells, *Developmental biology*, 2008, **322**, 406-414.
37. G. Carnac, B. Vernus and A. Bonniou, Myostatin in the pathophysiology of skeletal muscle, *Current genomics*, 2007, **8**, 415-422.
38. L. Yi, A. Donsante, M. L. Kennerson, J. F. Mercer, J. Y. Garbern and S. G. Kaler, Altered intracellular localization and valosin-containing protein (p97 VCP) interaction underlie ATP7A-related distal motor neuropathy, *Human molecular genetics*, 2012, **21**, 1794-1807.
39. L. Xie and J. F. Collins, Copper stabilizes the Menkes copper-transporting ATPase (Atp7a) protein expressed in rat intestinal epithelial cells, *American journal of physiology. Cell physiology*, 2013, **304**, C257-262.
40. D. J. Waggoner, T. B. Bartnikas and J. D. Gitlin, The role of copper in neurodegenerative disease, *Neurobiology of disease*, 1999, **6**, 221-230.
41. G. Tamiya, S. Makino, M. Hayashi, A. Abe, C. Numakura, M. Ueki, A. Tanaka, C. Ito, K. Toshimori, N. Ogawa, T. Terashima, H. Maegawa, D. Yanagisawa, I. Tooyama, M. Tada, O. Onodera and K. Hayasaka, A mutation of COX6A1 causes a recessive axonal or mixed form of Charcot-Marie-Tooth disease, *American journal of human genetics*, 2014, **95**, 294-300.
42. J. B. Hilton, A. R. White and P. J. Crouch, Metal-deficient SOD1 in amyotrophic lateral sclerosis, *J Mol Med (Berl)*, 2015, **93**, 481-487.
43. S. Y. Jeong, K. I. Rathore, K. Schulz, P. Ponka, P. Arosio and S. David, Dysregulation of iron homeostasis in the CNS contributes to disease progression in a mouse model of amyotrophic lateral sclerosis, *The Journal of neuroscience : the official journal of the Society for Neuroscience*, 2009, **29**, 610-619.
44. M. L. Schlief, A. M. Craig and J. D. Gitlin, NMDA receptor activation mediates copper homeostasis in hippocampal neurons, *The Journal of neuroscience : the official journal of the Society for Neuroscience*, 2005, **25**, 239-246.
45. M. L. Schlief, T. West, A. M. Craig, D. M. Holtzman and J. D. Gitlin, Role of the Menkes copper-transporting ATPase in NMDA receptor-mediated neuronal toxicity, *Proceedings of the National Academy of Sciences of the United States of America*, 2006, **103**, 14919-14924.
46. T. A. Mays, J. L. Sanford, T. Hanada, A. H. Chishti and J. A. Rafael-Fortney, Glutamate receptors localize postsynaptically at neuromuscular junctions in mice, *Muscle & nerve*, 2009, **39**, 343-349.
47. A. I. Malomouzh, L. F. Nurullin, S. S. Arkhipova and E. E. Nikolsky, NMDA receptors at the endplate of rat skeletal muscles: precise postsynaptic localization, *Muscle & nerve*, 2011, **44**, 987-989.
48. K. K. Walder, S. B. Ryan, T. Bzdega, R. T. Olszewski, J. H. Neale and C. A. Lindgren, Immunohistological and electrophysiological evidence that N-acetylaspartylglutamate is a co-transmitter at the vertebrate neuromuscular junction, *The European journal of neuroscience*, 2013, **37**, 118-129.

1
2
3 This conditional knock in mouse (*Atp7aT985I*) modelling the human X-linked distal
4 hereditary motor neuropathy (dHMNX) cellular phenotype is significant and of
5 interest to the metalloomics community. As the majority of mutations in an essential
6 Cu transporter (*ATP7A*) cause severe and systemic Menkes disease this study
7 highlights a unique situation where a specific *ATP7A* point mutation exclusively
8 causes a non fatal motor neuron disease. Our model will allow future investigations of
9 the subtle defects in Cu metabolism and transport within the nervous system and
10 provide the opportunity to further explore the impact of these pathogenic changes in
11 motor neurons.
12
13
14
15
16
17
18
19
20
21
22
23
24
25
26
27
28
29
30
31
32
33
34
35
36
37
38
39
40
41
42
43
44
45
46
47
48
49
50
51
52
53
54
55
56
57
58
59
60